ORIGINAL ARTICLE

Setomimycin as a potential molecule for COVID-19 target: in silico approach and in vitro validation

Ravi S. Manhas[1,5] · Harshita Tiwari[2,5] · Mateen Noor[3,5] · Ajaz Ahmed[2,5] · Jyoti Vishwakarma[4,5] · Raja B. M. Tripathi[4,5] · Ravishankar Ramachandran[4,5] · Sreedhar Madishetti[3,5] · Debaraj Mukherjee[2,5] · Amit Nargotra[2,5] · Asha Chaubey[1,5]

Abstract

COVID-19 pandemic caused by the SARS-CoV-2 virus has led to a worldwide crisis. In view of emerging variants time to time, there is a pressing need of effective COVID-19 therapeutics. Setomimycin, a rare tetrahydroanthracene antibiotic, remained unexplored for its therapeutic uses. Herein, we report our investigations on the potential of setomimycin as COVID-19 therapeutic. Pure setomimycin was isolated from *Streptomyces* sp. strain RA-WS2 from NW Himalayan region followed by establishing in silico as well as in vitro anti-SARS-CoV-2 property of the compound against SARS-CoV-2 main protease (M^{pro}). It was found that the compound targets M^{pro} enzyme with an IC_{50} value of 12.02 ± 0.046 μM. The molecular docking study revealed that the compound targets Glu166 residue of M^{pro} enzyme, hence preventing dimerization of SARS-CoV-2 M^{pro} monomer. Additionally, the compound also exhibited anti-inflammatory and anti-oxidant property, suggesting that setomimycin may be a viable option for application against COVID-19 infections.

Ravi S. Manhas, Harshita Tiwari have contributed equally to this work.

✉ Asha Chaubey
achaubey@iiim.res.in

✉ Amit Nargotra
anargotra@iiim.res.in

1 Fermentation & Microbial Biotechnology Division, CSIR-Indian Institute of Integrative Medicine, Canal Road, Jammu 180001, India

2 Natural Products & Medicinal Chemistry Division, CSIR-Indian Institute of Integrative Medicine, Canal Road, Jammu 180001, India

3 Pharmacology Division, CSIR-Indian Institute of Integrative Medicine, Canal Road, Jammu 180001, India

4 Division of Biochemistry and Structural Biology, CSIR- Central Drug Research Institute, Lucknow 226031, India

5 Academy of Scientific and Innovative Research, CSIR- Human Resource Development Centre, Campus Ghaziabad, Ghaziabad 201002, India

Graphical abstract
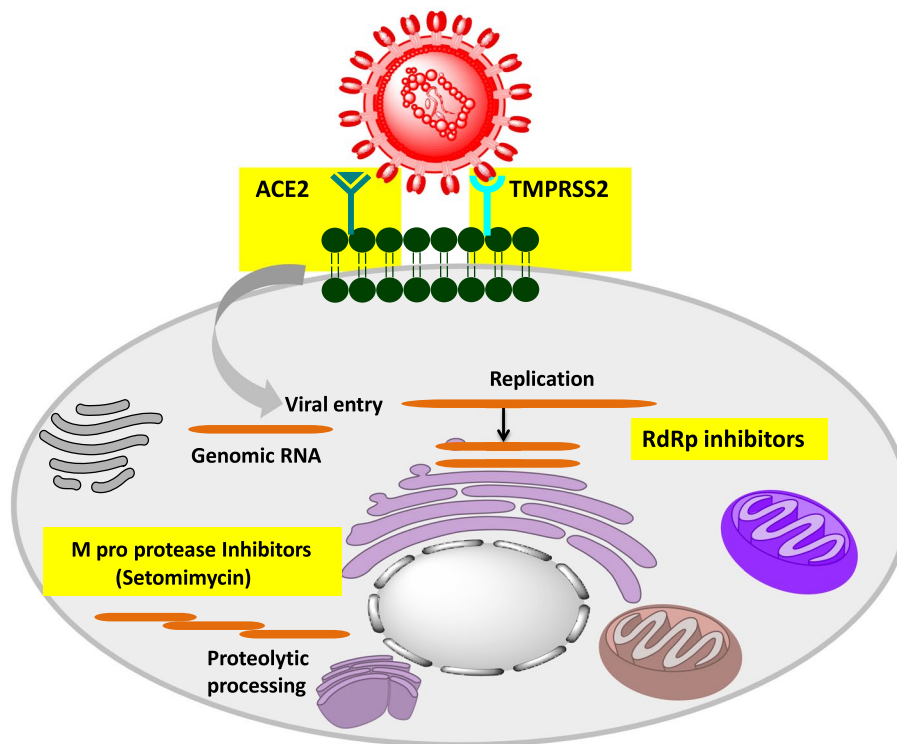
Keywords SARS-CoV-2 · COVID-19 target · In silico · Setomimycin · Main protease (M^{pro})

Introduction

Coronaviruses (CoVs) are a group of diverse enveloped positive-sense single-stranded RNA viruses that infect both animals other aves [1]. Human coronaviruses (HCoVs) are categorized into two types based on the frequency of spreading and severity, viz. those which are widespread and less severe (OC43, 229E, HKU1, and NL63) and those that are very infectious and severe (Severe Acute Respiratory Syndrome Coronavirus: SARS-CoV, Middle East Respiratory Syndrome Coronavirus: MERS-CoV, and Severe Acute Respiratory Syndrome Coronavirus-2: SARS-CoV-2) [2]. Over the last two decades, the three extremely infectious viruses SARS-CoV, MERS-CoV, and SARS-CoV-2 have caused a considerable number of fatalities in 2003, 2013, and 2019, respectively [3–5]. The recent SARS-CoV-2 pandemic has produced an unsettling scenario on a worldwide scale. During late 2019, the first case of SARS-CoV-2 was reported in the wet market of Wuhan city in China [6]. In March 2020, soon after global spread of the virus, the disease got pandemic status by World Health Organization (WHO) [7]. As of now, it has claimed almost 55 million lives worldwide.

SARS-CoV-2 is a pleomorphic beta virus containing ~30kb single-stranded RNA genome [8, 9]. This virus genome encodes two large overlapping polyprotein precursors, pp1a (4405 amino acids) and pp1ab (7096 amino acids), responsible for viral replication and transcription [10]. These polypeptides synthesize five structural proteins spike (S), envelope (E), membrane, nucleocapsid (M), and hemagglutinin-esterase dimer glycoproteins (HE), sixteen non-structural proteins nsp (PL^{pro}; nsp3, 3CLpro; nsp5 and RdRP; nsp12, etc.), and several auxiliary proteins [11]. Two viral cysteine proteases cleave these polyproteins into non-structural proteins: chymotrypsin-like main protease (M^{pro}) and papain-like protease (PL^{pro}) [12]. M^{pro} is a 33.8 kDa enzyme that digests the polyprotein at 11 conserved sites. M^{pro} is unique in that it cleaves polypeptides solely after a glutamine (Gln) residue, a cleavage specificity shared by no other human protease [13]. PL^{pro} is a 35.6 kDa enzyme that catalyzes the cleavage of the polypeptide at three distinct sites. Along with proteolytic action, it also performs the deubiquitinating and deISG15ylating (interferon-induced gene 15) activities [14]. These viral proteases are therefore important antiviral targets due to their critical involvement in viral replication and maturation [14, 15]. RNA-dependent RNA polymerase (RdRP/ nsp12) is an important part of the virus replication and transcription complex. Along with the cofactors, nsp7 and nsp8 aid the viral replication and

transcription. RdRP is highly specific among RNA viruses, hence representing a good starting point for antiviral drug discovery [16]. Furthermore, structural viral proteins are also important for viral survival, infectivity, and transmissibility [17]. Spike protein is crucial for the entry of the virus into host cells. The cellular transmembrane serine protease (TMPRSS2) cleaves the spike protein into unique polypeptides; S1 and S2.S1 and S2 polypeptides are essential for anchoring virus to the cellular receptor ACE2 and for membrane fusion. The TMPRSS2 is highly expressed in the cell surface of nasal, bronchial, and gastrointestinal epithelium. The antibodies developed in COVID-19 patients were neutralized by the membrane protein (M). The transmembrane envelope protein (E) functions as an ion channel and is required for viral genetic material to be released into the host cell. Although the protein is not required for viral replication, it facilitates pathogenicity by allowing the virus to be assembled and released. The nucleocapsid protein (N) aids in the viral genome encapsulation into virus particles by attaching the viral genome network of proteins to the replicase-transcriptase complex (RTC) machinery. Acetyl-esterase activity found in the hemagglutinin-esterase dimer protein (HE) helps it in attachment and detachment from the host. The drugs that are investigated for COVID-19 work by inhibiting one of these critical proteins, viz. remdesivir, sofosbuvir, etc. (SARS-CoV-2 RdRp inhibitor), protease inhibitors, i.e., lopinavir, ritonavir, etc. (SARS-CoV-2 M^pro), camostat mesilate (TMPRSS-2 inhibitor), etc. Thus, targeting proteins essential for viral lifecycle is an important strategy for curing COVID-19 disease [18–21]. However, despite numerous efforts worldwide, options for COVID-19 therapy are still limited.

Following viral entry, the first inflammatory reaction drives the recruitment of virus-specific T lymphocytes. The recruited virus-specific T lymphocytes kill infected cells before the virus spreads, resulting in recovery of the majority of patients. However, the virus generates an atypical host immune reaction in individuals with severe SARS-CoV-2 infections. These responses result in pathological condition known as acute respiratory distress syndrome (ARDS) characterized by inflammation, alveolar damage, hyaline membrane formation, interstitial mononuclear inflammatory infiltrates [22]. In contrast with SARS and MERS, COVID-19 patients have mucus plugs in the respiratory tract with fibrinous exudate because of an excess of pro-inflammatory cytokines accumulating in the lungs and finally causing lung tissue destruction. If the immune response continues to deteriorate and cytokines accumulate in other organs, severe tissue damage or a cytokine release syndrome (cytokine storm) may result in capillary leakage, thrombus development, and organ failure [23]. At this stage, immunosuppressive drugs such as tocilizumab and anti-inflammatory corticosteroids

reported to be effective therapy to prevent lung injury and organ damage [24].

Therapeutics for COVD-19 disease can be discovered/repurposed by two main approaches, i.e., experimental (high throughput screenings) and computational methodologies (virtual screening) [25–27]. Experimental approaches to find COVID-19 therapeutics are costly and time-consuming process. Computational approaches provide a number of benefits over experimental methods, including the ability to drastically reduce the cost and time associated with the drug development process [28]. Additionally, the availability of a huge amount of data linked to COVID-19 disease in the public domain facilitated the deployment of several in silico drug development approaches [29].

The aim of present research was to examine setomimycin, a rare tetrahydroanthracene antibiotic for its therapeutic potential against COVID-19. Setomimycin was first isolated in 1978 from *Streptomyces pseudovenezuela* with in vitro antibacterial activity and in vivo antitumor activity [30]. Further, few compounds of the same class were isolated from different actinobacteria; however, this antibiotic remains unexplored for commercial exploitation. Therefore, efforts were made by our group to isolate and purify setomimycin from a new source. Subsequently, the binding potential of setomimycin was investigated with COVID-19 targets including M^pro, S protein-ACE2 complex, RdRp, and TMPRSS2 using molecular docking studies.

Following the in silico study, in vitro evaluation of the compound was carried out against the target (M^pro) suggested by molecular docking studies. Additionally, the anti-inflammatory and antioxidant activity of the antibiotic was also evaluated to support the evident use of setomimycin as a potential anti-COVID-19 drug candidate.

Materials and methods

Source of setomimycin and fermentation conditions

The actinobacterium used in the present study was isolated from a soil sample of the Shivalik region of NW-Himalayas. Freshly grown culture of *Streptomyces* sp. isolate RA-WS2 was inoculated into 250-ml Erlenmeyer flask containing 50 ml of pre-seed medium (constituents in g/L: soluble starch 25.0, soyabean meal 15.0, calcium carbonate 4.0, and yeast extract 2.0; pH 6.8) and was grown at 28 °C and 200 rpm on a rotary shaker. Two days old pre-seed culture was transferred to 1-L Erlenmeyer flasks containing 250 ml of the same medium to prepare seed inoculum. 10% of two-day-old seed inoculum was transferred to a 7-L fermenter containing a 4-L production medium having constituents same as that of pre-seed and seed medium. The fermentation

was carried out at 28 °C and 100 RPM with 0.5 vvm air for 6 days.

Preparation of solvent extract

After fermentation for 6 days in production medium, broth was homogenized with 10% methanol for about two hours. The solvent (ethyl acetate) was added in a ratio of 1:1(v:v) and vigorously shaken for 20 min. The ethyl acetate phase that contains antibiotic was separated from the aqueous phase using separating funnel. The process was repeated three times to obtain all the extractable constituents. Solvent fraction was concentrated by evaporation under vacuum at 50 °C to obtain dry extract [31].

Activity guided isolation of setomimycin

The crude solvent extract obtained above was subjected to thin layer chromatography and observed under UV. Antimicrobial activity on TLC was evaluated by the method described by Rahalison et al. [32]. Various fractions were evaluated for activity against *Staphylococcus aureus,* and active fractions were further purified by preparative TLC to obtain setomimycin. The structure of the isolated compound was confirmed by PMR and CMR spectroscopy and submitted to institutional compound repository (IN00664).

Anti-SARS-CoV-2 activity of setomimycin

Molecular Docking Studies of setomimycin with selected targets

Four therapeutic targets, i.e., SARS-CoV-2 M^{pro} (PDB ID: 6LU7), SARS-CoV-2 S-protein- ACE2 complex (PDB ID: 6M17), SARS-CoV-2 RdRp/NSP12 (PDB ID: 6NUR), and transmembrane protease, serine 2 (TMPRSS2), were selected for molecular docking studies [33–35]. The three-dimensional structure coordinates of all the targets were retrieved from Protein Data Bank (PDB) except TMPRSS2. The homology model of TMPRSS2 was downloaded from the SARS-CoV-2 repository of SWISS-MODEL [36]. The structure was built using serine protease hepsin as a template and showed Q Mean score is -1.62 for the modeled structure. Before docking studies, all the proteins structures were prepared with Protein preparation wizard of Schrödinger 2017–3 suit [37]. This stage included the addition of missing hydrogen bonds, the assignment of bond ordering, and the energy minimization of the structure using the OPLS3e force field.

Ligand dataset preparation

The three-dimensional structures of setomimycin and other selected standard compounds were downloaded from the PubChem database [38–43]. The prodrugs favipiravir, remdesivir, and ribavirin were converted to active form for the study. Prior to molecular docking, all the compounds were prepared with LigPrep module [37, 44].

Molecular docking studies

The active site/receptor grids were generated with the receptor grid generation module. For SARS-CoV-2 M^{pro}, the active site was predicted with the sitemap module [45]. After sitemap prediction, the site showing best site score was selected for grid generation. For SARS-CoV-2 Sprotein-ACE2 complex, interface of SARS-CoV-2 S-protein and ACE2 interface were used for grid generation. The residues of SARS-CoV-2 S-protein found in the 5 Å proximity of ACE2 are Arg403, Gly446, Tyr449, Tyr453, Leu455, Phe456, Tyr473, Ala475, Gly476, Ser477, Phe486, Asn487, Tyr489, Gln493, Tyr495, Gly496, Gln498, Thr500, Asn501, Gly502, Tyr505. Molecular grid in SARS-CoV-2 RdRP was generated using the binding site of the drug sofosbuvir. Although the drug sofosbuvir was found to inhibit RdRP enzyme, the crystal structure information was not available [44]. Since the catalytic site of SARS-CoV-2 and Hepatitis C virus (HCV) RdRp is structurally conserved, it was assumed that the drug will bind to the similar residues on the COVID-19 virus [46]. Therefore, the HCV RdRp in complex pp-sofosbuvir (PDB ID 4WTG) was superimposed on SARS-CoV-2 RdRp. The grid was generated around the superimposed active site of SARS-CoV-2 and HCV RdRp [47, 48]. The TMPRSS2 active site was also predicted using the sitemap module. Because the active site of serine proteases consists of amino acid residues His 296, Asp345, and Ser441, the site containing the catalytic triad was selected to generate the molecular grid.

All molecular docking experiments were carried out using Schrödinger glide (Grid-Based Ligand Docking with Energetics) program in extra precision (XP) mode [49]. After molecular docking, the docking scores and interaction of setomimycin and standard compounds were compared.

Molecular dynamic (MD) simulation

Molecular dynamics (MD) simulation studies of the setomimycin-SARS-CoV2-M^{pro} were carried out using Desmond 2018–3 [50]. The MD simulation was initiated with the best docking pose of setomimycin with M^{pro}. The system was solvated with three point (TIP3P) water model and neutralized by adding Cl$^-$ or Na$^+$ counter ions in an orthorhombic box (10 Å × 10 Å × 10 Å). Before the MD simulation,

system was minimized via Steepest descent energy minimization method till 2000 iterations. The 50 ns MD simulation was performed with NPT condition. Finally, the generated trajectories were analyzed to obtain root-mean-square deviation (RMSD), root-mean square fluctuation (RMSF), protein–ligand interaction, protein–ligand contacts, and radius of gyration using simulation interaction diagram utility.

Principal component analysis

Principal component analysis (PCA) was performed to understand the correlated motions of the residues. The PCA was performed using ProDy implemented using normal mode wizard (NMW) of VMD software [51, 52]. For the calculation of the principal components describing the conformational dynamics, the covariance matrix of the C-α atoms of M^{pro} protein was used. The PCA scatter plots of the major components were generated using the plotly Python library (https://plotly.com/).

MMGBSA energy calculations

After MD simulation, the average binding free energy (dG_bind) was estimated with the molecular mechanics-generalized born surface area (MM-GBSA) analysis [53]. The MMGBSA calculation was performed on 200 complexes by extracting each tenth frame of the last 10 ns of stable trajectory with thermal_mmgbsa.py script provided by Schrodinger [54]. The formula used for binding free energy is as follows:

$$\Delta G(binding) = \Delta G(complex) - \Delta G(protein) - \Delta G(ligand)$$

In vitro protease activity assay

In order to validate in silico observations, in vitro activity of setomimycin against main protease (M^{pro}) was performed. For M protease proteolytic assay, the fluorogenic substrate DABCYL-KTSAVLQSGFRKME-EDANS was custom synthesized (Thermo Fisher scientific). The protease assay was performed in fluorescence spectrophotometer (Cary Eclipse, Agilent Technology) 1-ml cuvette with final reaction volume of 400 µl at room temperature; 750 nM M^{pro} recombinant protein and various concentrations of setomimycin (1.5, 3.25, 6.125, 12.5, 25,50 M) were incubated for 20 min in reaction buffer (50 mM Tris–HCl pH 8.0, 1 mM DTT, 1 mM EDTA). The substrate with final concentration of 25 µM was added to the reaction mixture and incubated for 40 min at room temperature. The same compound concentration with substrate and without M^{pro} was used as blank. The fluorescence signal of released EDANS was measured by excitation at 360 nm and emission at 490 nm. The IC_{50} values

of setomimycin were determined by GraphPad Prism 5.0 using nonlinear regression dose–response inhibition with a variable slope.

In vitro anti-inflammatory activity

Cell culture

RAW 264.7 macrophage cells were grown in Dulbecco's Modified Eagle Medium (DMEM; GIBCO) containing 10% fetal bovine serum (FBS), 100U/mL penicillin, and 100 ng/mL streptomycin. The process was followed by incubation at 37 °C under 5% CO_2.

Cytokines estimation

To quantify cytokines (TNF-α, IL-1β or IL-6), an ELISA assay (using Invitrogen ELISA kit) was carried out according to the manufacturer's instructions. To conduct the assay, 96-well plates were seeded with RAW 264.7 cells (1lac cells /well). Following overnight incubation, the cells were treated with setomimycin (1.0, 0.3, 0.1, 0.03, and 0.01 µM) and standard dexamethasone (10 µM) for 1 h. The treated cells were incubated with 1 µg/ml LPS for 24 h. After 24 h, the supernatants were collected and kept at -80 °C until analysis. The concentration of the cytokines TNF-α, IL-1β, or IL-6 in the samples was quantified using a standard curve. The data have been shown as the mean (of quadruplicate determinations) $\pm$ standard error of the mean. The formula used to calculate the percent inhibition is given below:

$$\text{Inhibition } (\%) = ((C - D)/C) * 100$$

wherein C represents cytokine concentration of LPS alone treated cells supernatant; D represents cytokine concentration of cells supernatant pretreated with test sample followed by stimulation with LPS.

Measurement of nitric oxide (NO assay)

For NO assay, RAW 264.7 macrophage cells were treated with setomimycin (1, 0.3, 0.1, 0.03, and 0.01 µM), dexamethasone (10 µM) and positive control L-NAME (100, 10 & 1 µM) and incubated for 1 h. After the incubation, 1 µg/ml LPS was added and the sample was again incubated for 24 h. After overnight incubation, the cell culture supernatants were collected and used for the nitrite concentration was determined using Greiss reagent (1% sulfanilamide/0.1% naphtylethyenediamine dihydrochloride in 2.5% H_3PO_4) as per manufacturer's instructions. Briefly, equal volumes of cell culture supernatant and griess reagent were mixed. After 10 min at room temperature, the

absorbance was measured at 540 nm using Spectramax ABS Plus microplate reader (Molecular Devices). A sodium nitrite standard curve was used to estimate the concentration of nitrite in the samples. The data provide mean (of quadruplicate determinations) ± standard error of the mean. The nitric oxide (NO) inhibition (%) was calculated as follows

$$\text{NO inhibition } (\%) \ = \ ((E - F)/E) * 100$$

wherein E represents the concentration of NO in the supernatant collected from LPS only treated cells and F represents NO concentration of cells supernatant pretreated with test sample followed by LPS.

Antioxidant activity of setomimycin

The antioxidant potential of the compound was measured using 2,2-diphenyl-1-picryl-hydrazyl-hydrate (DPPH) free radical method. For the experimentation, the method described by Xie et al. was used with slight adjustments [55–57]. Briefly, for the assay the DPPH solution was prepared by adding180 μL of methanol to the 10 μL of 1 mg/ml solution of DPPH. To this DPPH solution, 10 μL of different concentrations of test sample/standard was added. The absorbance of the solutions was measured at 60 min time point at 515 nm with Spectramax ABS Plus microplate reader (Molecular Devices). Ascorbic acid and quercetin were used as standard at a concentration range of 150 to 0.11 μM, and setomimycin was used at a concentration range of 500 to 0.36 μM. The following equation was used to measure free radical scavenging activity (DPPH inhibition)

$$\text{DPPH inhibition } (\%) \ = \ ((A - B)/A) * 100$$

wherein A is the DPPH solution's absorbance, B the DPPH solution added with sample's absorbance.

Cytotoxicity evaluation using MTT assay

The cytotoxicity of the compound was measured with 3-(4,5-dimethylthiazol-2-yl)-2,5-diphenyltetrazolium bromide (MTT) assay. For cytotoxicity determination, RAW 264.7 macrophage cells were treated for 48 h with either test samples or camptothecin (10 μM—used as standard) or vehicle. After the treatment, the cells were incubated for 4 h with MTT solution (2.5 mg/ml). The incubation is followed by removal of supernatant, addition of DMSO to solubilize the formazan crystals, and determination of absorbance at 570 nm using Spectramax ABS Plus microplate reader (Molecular Devices). The data represent the mean (of quadruplicate) ± standard error of the mean. The % cell viability was calculated as follows

$$\% \text{ cell viability } \ = \ (\text{treated cells absorbance}/ \text{ untreated cells absorbance}) * 100$$

Results and discussion
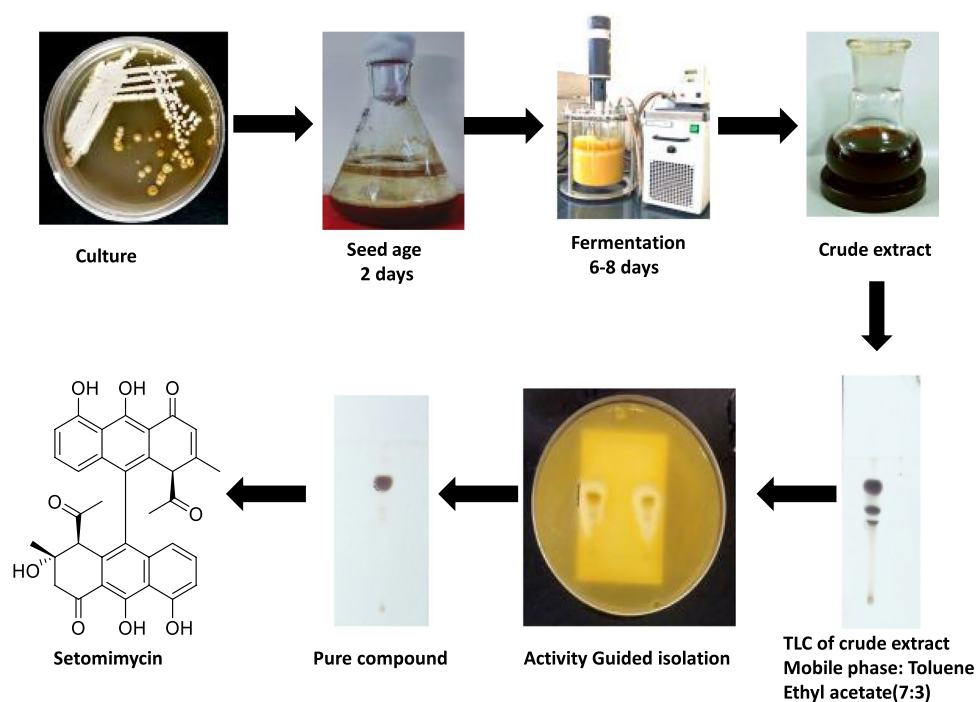
Fermentation and production of setomimycin

The setomimycin-producing *Streptomyces* strain used in the study presented potent antimicrobial activity against *Bacillus cereus* and *Staphylococcus aureus* during preliminary experiments. Production of the setomimycin was carried out by fermentation of *Streptomyces* sp. RA-WS2 strain under specified conditions (as stated in the materials & methods section) for 6 days. After termination of fermentation batch, the fermented broth was homogenized with 10% MeOH followed by extraction with 1:1(v:v) ethyl acetate. In order to extract all the bioactives, the broth was extracted at least thrice with ethyl acetate. A mobile phase of ethyl acetate in hexane (1:1) was used to run the TLC for the separation of crude extract constituents and observed under UV. The TLC was further subjected to antimicrobial activity against *S. aureus* to observe the zone of inhibition and the major spot showing zone of inhibition was scratched to get pure compound (Fig. 1).

Characterization of pure compound

The pure compound from preparative TLC was obtained as a red solid with the molecular mass of 580.0 as determined by LCMS fragmentation. The PMR spectra suggest that the compound contains 28 protons: 12 protons from 4 methyl groups, 2 protons from a methylene group, 2 protons from two C-H, 7 protons from olefinic and/or aromatic moieties, and 5 protons from 5 hydroxyl groups, and in CMR, 34 carbons were found, 4 in carbonyl region, 5 in aromatic with substitution, 17 in aromatic, 3 in the oxygenated region, 1 in methylene, and 4 in methyl region. IR spectra revealed that the compound contains C=C and hydroxyl groups. By calculating the 21 degrees of unsaturation and UV absorptions of the compound, it indicates that it contains naphthocyclinone or anthracyclinone skeleton as a chromophore and it contains no sugar moiety.

^{1}H NMR (400 MHz, CDCl$_3$) δ 10.04 (s, 1H), 9.93 (s, 1H), 7.33 (t, J = 8.0 Hz, 1H), 7.22 – 7.15 (m, 2H), 6.93 (d, J = 7.8 Hz, 1H), 6.83 (d, J = 7.9 Hz, 1H), 6.59 (d, J = 8.3 Hz, 1H), 6.21 (d, J = 7.5 Hz, 2H), 3.94 (s, 1H), 3.63 (s, 1H), 3.12 (d, J = 17.6 Hz, 1H), 2.58 (d, J = 17.8 Hz, 1H), 1.95 (s, 3H), 1.63 (s, 3H), 1.34 (s, 3H), 1.22 (s, 3H). **^{13}C NMR (101 MHz, CDCl$_3$)** δ 208.5, 203.3, 199.6, 191.1, 166.5, 164.8, 158.8, 158.5, 158.1, 138.7, 137.0, 134.3, 133.9, 133.5, 133.2, 125.8, 125.1, 124.3, 117.5, 116.5, 114.1,

Fig. 1 Scheme showing isolation of setomimycin from *Streptomyces* sp. RA-WS2 strain

Culture

Seed age
2 days

Fermentation
6-8 days

Crude extract

Setomimycin

Pure compound

Activity Guided isolation

TLC of crude extract
Mobile phase: Toluene
Ethyl acetate(7:3)

113.4, 113.0, 112.6, 112.5, 109.3, 108.6, 72.1, 60.9, 60.6, 47.2, 33.9, 29.4, 28.2, 23.0.

The analysis of NMR spectra characterized the pure compound as 1,1'-diacetyl-2,5,5',10,10'-pentahydroxy-2,2'-dimethyl-2,3-dihydro-[9,9'-bianthracene]-4,4'(1H,1'H)-dione a 9,9' bianthryl antibiotic known as setomimycin.

Anti-SARS-CoV-2 activity of setomimycin

Molecular docking studies of setomimycin with selected targets

The activity of setomimycin against selected targets was assessed using a molecular docking study. Setomimycin exhibited the best docking score with SARS-CoV-2 main protease (− 7.462 kcal/mol) among all the selected targets (Table 1). The docking score of setomimycin was comparable to the docking score of standard protease inhibitor lopinavir (-7.953 kcal/mol) and nelfinavir (− 7.884) (Table 1). From the 2D interaction diagrams, it was observed that all the compounds were interacting with Glu166 via hydrogen bonding (Fig. 2). Because Glu166 is required for dimerization of SARS-CoV-2 M^{pro} monomers, compounds targeting this residue will inhibit catalytic activity of the enzyme [58]. Setomimycin formed three hydrogen bonds with Glu166 and one each with Asn142 and Gly143 (Fig. 2 A-G). The findings show that setomimycin may efficiently inhibit M^{pro} to prevent SARS-CoV-2 infections. Therefore, SARS-CoV-2 main protease was selected as potential target for in vitro study.

Table 1 Docking score (kcal/mol) of compounds with selected targets

Compound	6LU7	6M17	6NUR	TMPRSS2
Setomimycin	− 7.462	− 6.192	− 5.877	− 6.638
Azithromycin	− 3.416	− 4.259	− 6.931	− 4.353
Lopinavir	− 7.953	–	–	–
Ritonavir	− 5.532	–	–	–
Darunavir	− 8.226	− 4.696	–	–
Nelfinavir	− 7.884	–	–	–
ATN-161	–	− 8.087	–	–
RBD-11b	–	− 6.719	–	–
Favipiravir-RTP	–	–	− 7.934	–
Remdesivir triphosphate	–	–	− 8.197	–
Ribavirin	–	–	− 8.664	–
Camostat mesylate	–	–	–	− 7.164
Nafamostat	–	–	–	− 9.470

Molecular dynamic (MD) simulation

To understand the behavior of the identified hit setomimycin in the dynamic system, 50 ns molecular dynamics simulation of setomimycin-SARS-CoV2-M^{pro} was performed. From the RMSD diagram, it can be inferred that the protein and inhibitor remain stable throughout the simulation time (Fig. 3A). The RMSF analysis confers that the M^{pro} remains stable in the presence of setomimycin (RMSF 0.4–4 Å) (Fig. 3B). The protein–ligand interaction diagram (Fig. 3C) showed the hydroxyl groups of setomimycin interacted
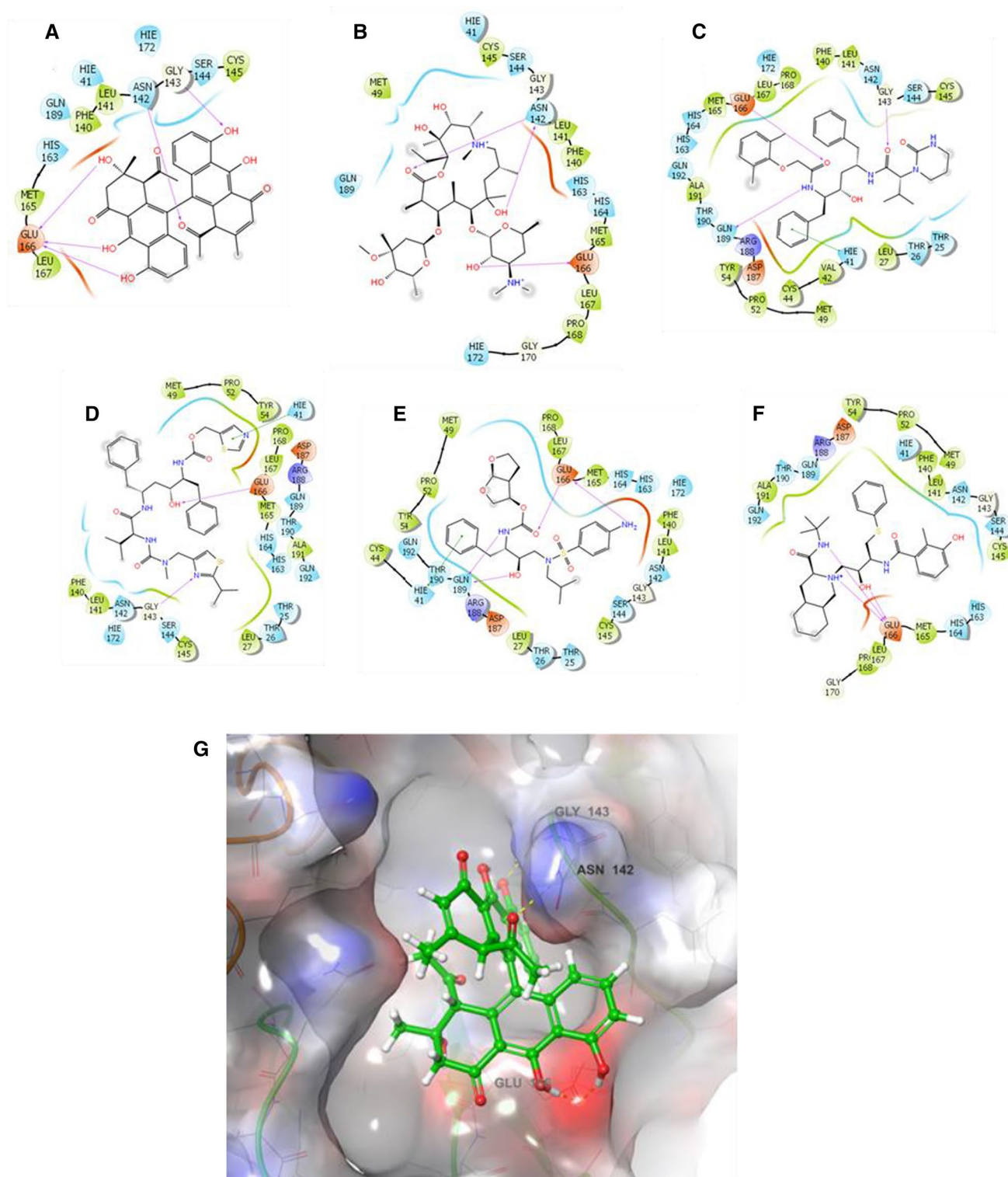
Fig. 2 2D interaction diagram of setomimycin (**A**) and standard compounds azithromycin (**B**), lopinavir (**C**), ritonavir (**D**), darunavir (**E**), and nelfinavir (**F**) to SARS-CoV-2 main protease. 3D interaction diagram of setomimycin bound to M^pro (**G**)

with the Ser144 and Glu166 via direct and water mediated hydrogen bonding interactions, respectively. Additionally, Thr26 and Glu166 interacted with the carbonyl oxygen via water-mediated and direct hydrogen bonds, respectively. Moreover, setomimycin interacted with Glu166 throughout the simulation (Fig. 3D). All, these interactions, might be
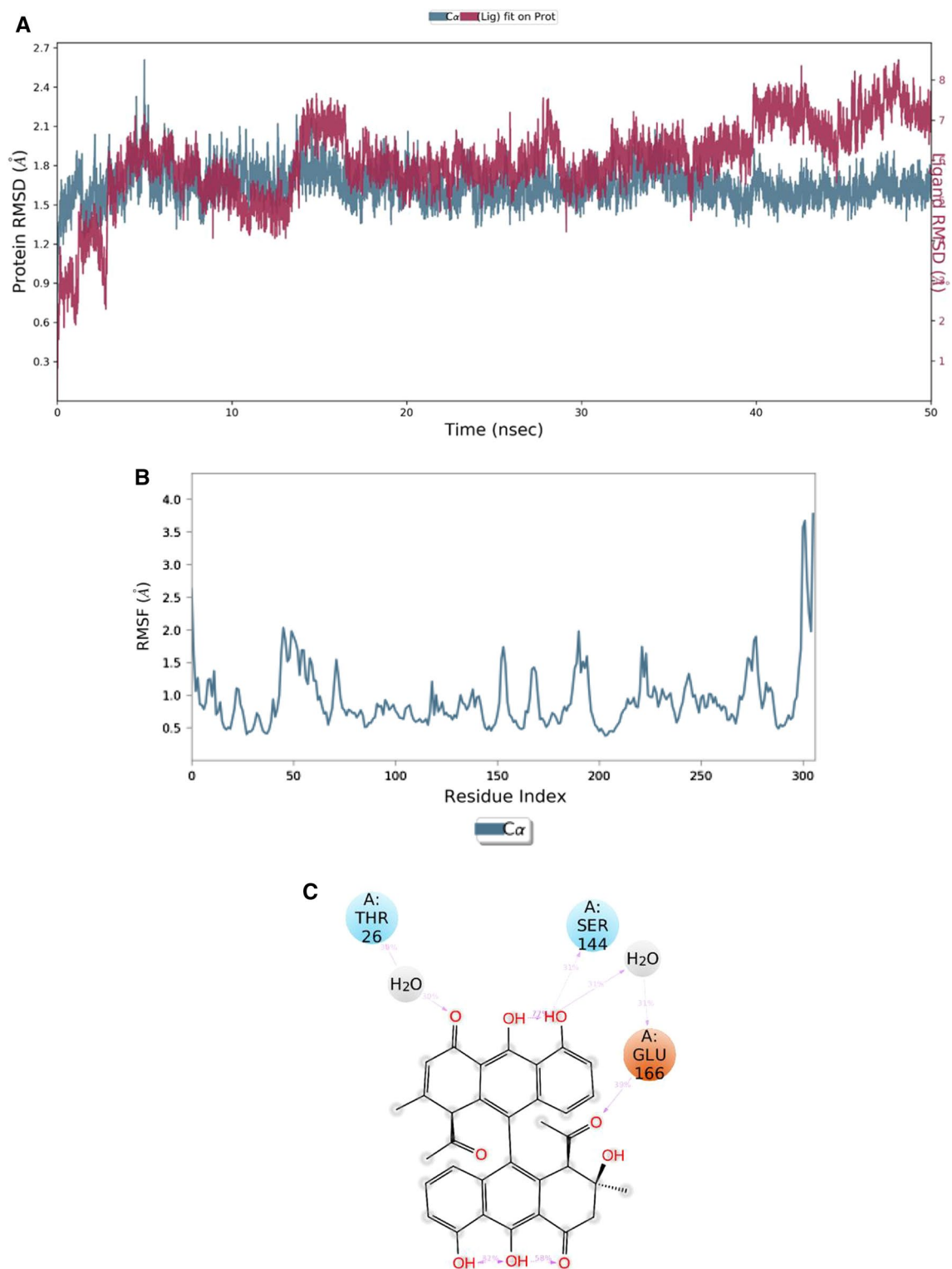
Fig. 3 **A** Root mean square deviation, **B** root mean square fluctuation of SARS-CoV-2 M^pro Cα and inhibitor setomimycin during 50 ns of MD simulation. **C** SARS-CoV-2 M^pro–setomimycin 2D interaction diagram. The interactions persisting more than 30% of total simulation time were shown. The pink arrow indicates hydrogen bonding interaction. **D** M^pro-setomimycin interactions (H-bonds, Hydrophobic, Ionic, Water bridges) during 50 ns simulation. The residues exhibiting interaction with more than one contact with the ligand are shown in a darker shade of orange. **E** Radius of gyration of ligand
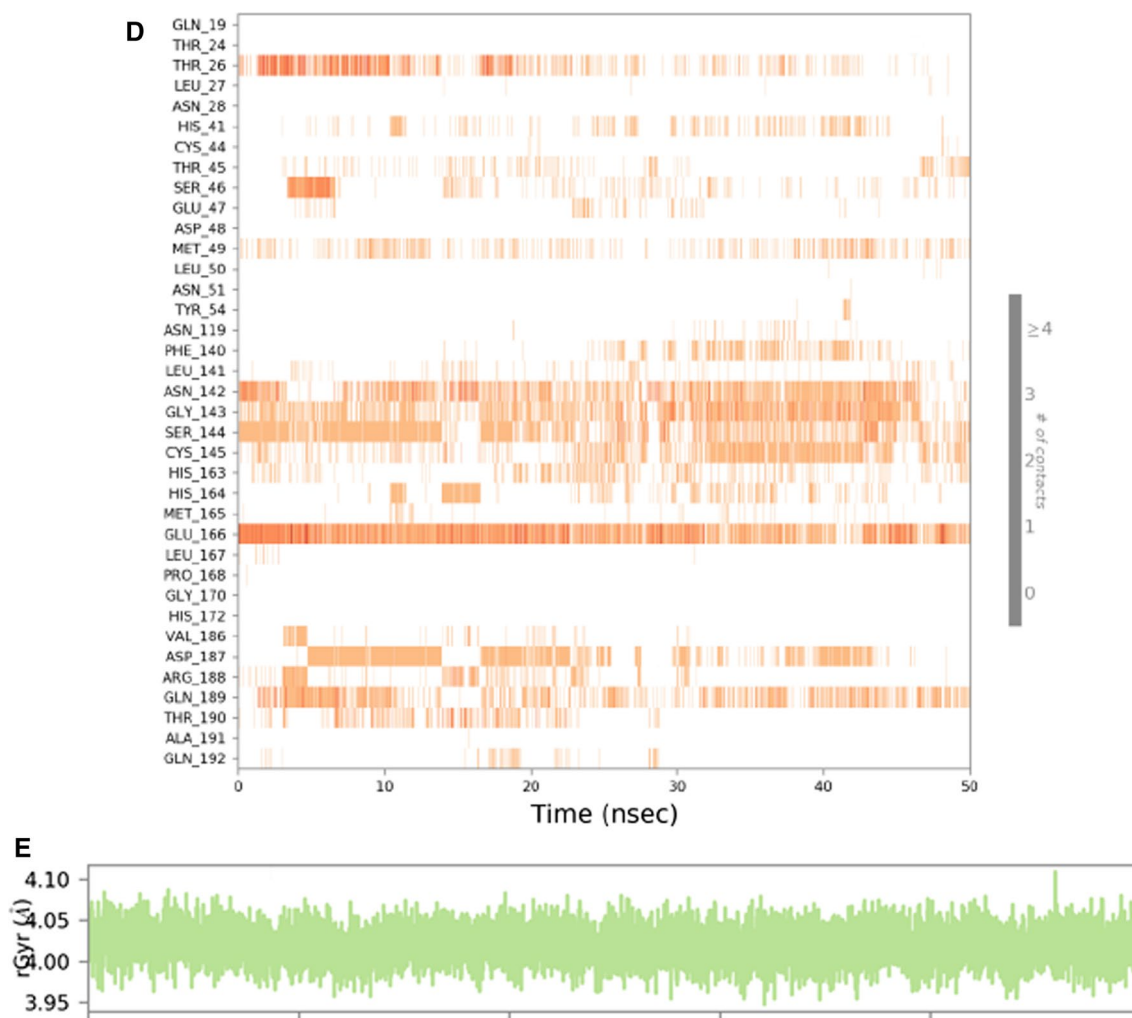
Fig. 3 (continued)

critical for the stable binding of setomimycin with SARS-CoV-2-M^{pro} enzyme. The radius of gyration of ligand was observed to within 5 Å, depicting compactness of the ligand during simulation (Fig. 3E).

Principal component analysis

The porcupine plots of PC mode 1 and mode 2 generated with normal mode wizard for capturing the dynamics revealed the local changes in the dynamics (Fig. 4A, B). The PCA scatter plot of the final trajectory obtained after 50 ns simulation is shown in Fig. 4C.

MMGBSA energy calculations

MMGBSA calculations demonstrate that setomimycin has a binding free energy (dG_Bind) of − 71.864 kcal/mol. It was also found that the van der Waals binding energy

(dG_Bind_vdW) of -42.381 kcal/mol was the major contributor to the binding. The main energy contributors are shown in Table 2.

In vitro protease activity assay

For the determining setomimycin potential to inhibit SARS-CoV-2 M^{pro} enzyme, fluorescence resonance energy transfer (FRET) enzymatic assay was performed. In this study, we found that setomimycin inhibited M^{pro} enzyme with half-maximum inhibitory concentration (IC$_{50}$) of 12.02 ± 0.046 µM (IC$_{50}$) (Fig. 5).

In vitro anti-inflammatory activity assay

Cytokines estimation

Pretreatment of RAW 264.7 cells with setomimycin in the concentration range of 0.01 to 1 µM resulted in the

Fig. 4 A Procupine plot depicting the motion of M^pro bound to setomimycin along PCA mode 1 (green arrow). **B** PCA mode 2 (red arrow) and 2D and **C** PCA scatter plot along with two principal components, principal component -1 and principal component -2
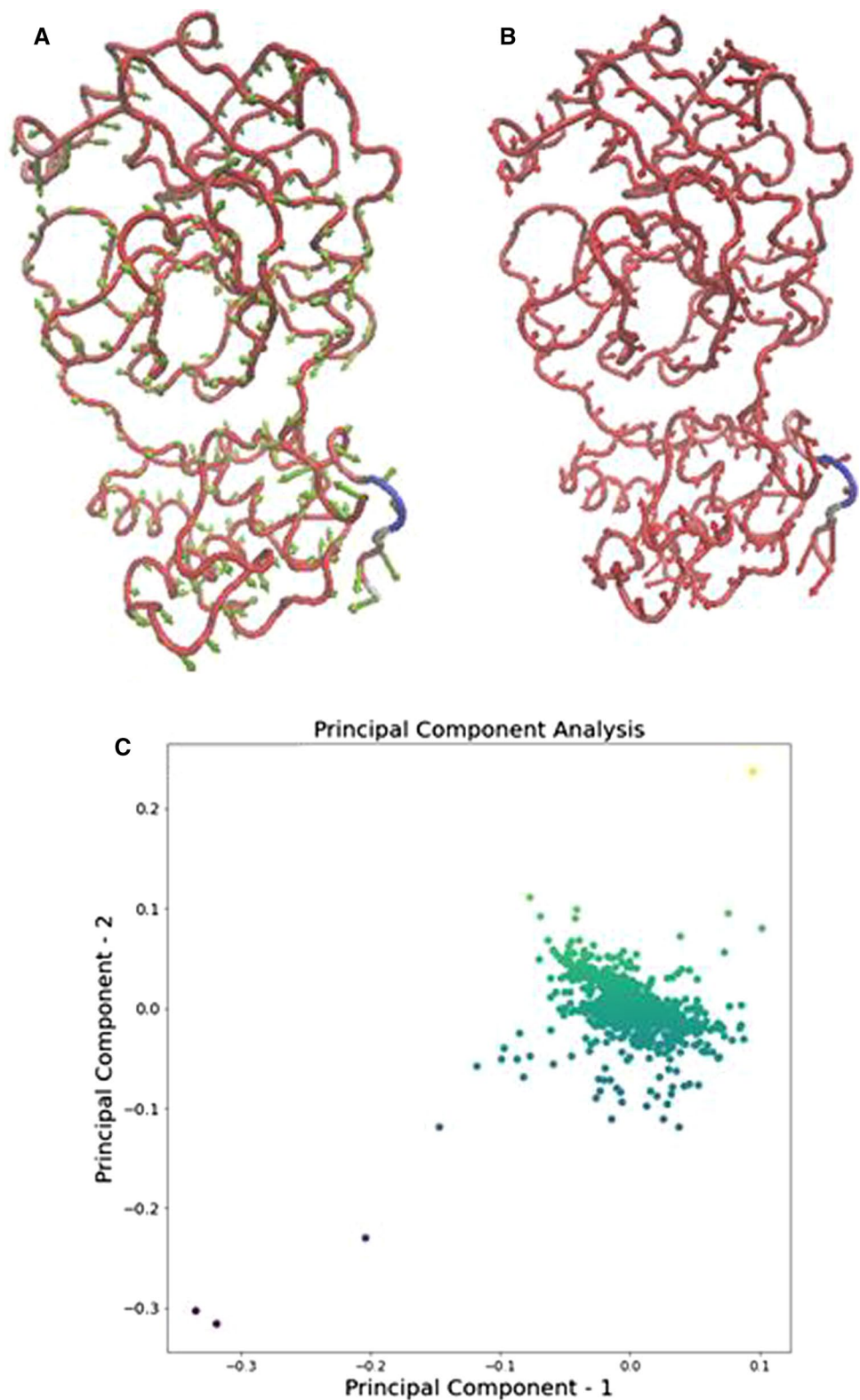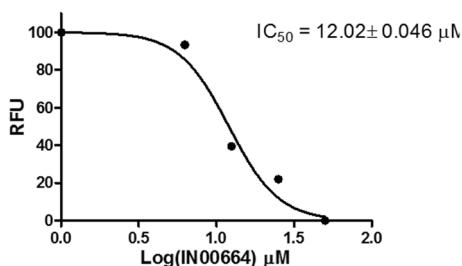

inhibition of the release of cytokines IL-1β, IL-6 and TNF-α from LPS stimulated RAW 264.7 cells in a dose-dependent manner comparable to standard drug dexamethasone (Fig. 6A–C).

Measurement of nitric oxide (NO assay)

Our results reveal that setomimycin pretreatment resulted in the reduction in LPS stimulated nitric oxide release.

Table 2 Average binding free energies (kcal/mol) of the setomimycin-SARS-CoV2-M^{pro}

Average binding free energy (dGBind)	Average van der Waals (dG_Bind_vdW)	Average Coulomb energy (dG_Bind_Coulomb)	Average hydrogen binding energy (G_Bind_Hbond)	Average lipophilic binding energy (dG_Bind_Lipo)
− 71.864	− 42.381	− 22.624	− 0.833	− 31.091

Fig. 7 Effect of setomimycin on nitric oxide release from LPS-induced RAW 264.7 cells

Fig. 5 IC$_{50}$ of setomimycin (IN00664) for in vitro M^{pro} inhibition assay

Setomimycin (0.01 to 1 μM) as well as positive control L-NAME (1–100 μM) inhibited NO release in a dose-dependent manner (Fig. 7).

Antioxidant activity of setomimycin

Setomimycin has shown good anti-oxidant properties (as measured by the potential to scavenge DPPH free radicals) with maximum activity of around 71% achieved at 500 μM following 60 min incubation. The DPPH inhibition shown was concentration dependent. Ascorbic acid and quercetin showed concentration-dependent increase in free radical

scavenging in the range of 0.011 to 150 μM. Ascorbic acid and quercetin showed around 90% inhibition of DPPH absorbance at 150 μM (Fig. 8).

Effect of setomimycin on viability of RAW 264.7 cells using MTT assay

RAW 264.7 cells treated with setomimycin in the concentration range of 0.15 to 1.25 μM for 48 h did not show appreciable cell death confirming that at these concentrations setomimycin was not toxic to cells (Fig. 9). This in turn confirms that the cytokine inhibition and nitric oxide inhibition of setomimycin were not due to cytotoxicity.

Conclusions

Despite enormous tireless efforts of the scientific community, COVID-19 infection continues to result in significant morbidity and mortality. Although several prospective
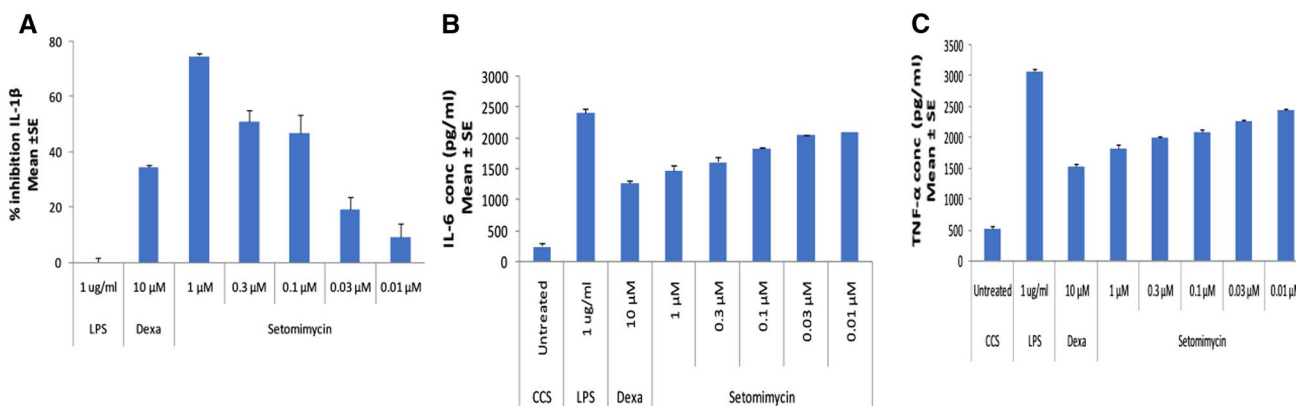
Fig. 6 Effect of setomimycin on cytokine **A** IL-1 β, **B** IL-6, and **C** TNF-α release from LPS-induced RAW 264.7 cells
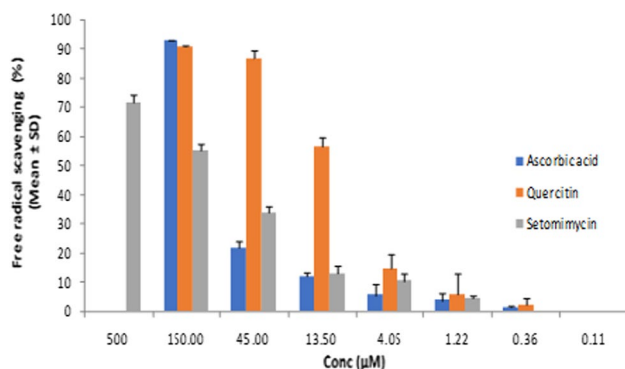
Fig. 8 Antioxidant activity of setomimycin, ascorbic acid, and quercetin using DPPH as free radical following 60 min incubation
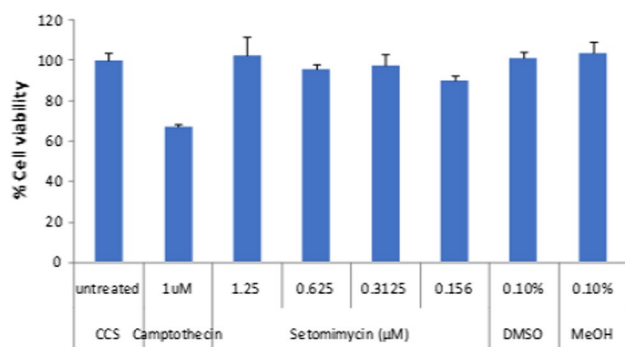

Fig. 9 Effect of setomimycin on viability of RAW 264.7 cells

therapies have been proposed, World Health Organization has approved remdesivir, for the treatment of COVID-19, and several are under trial. Due to emergency health conditions, treatments for COVID-19 illness are gravely needed to alleviate the socioeconomic implications of the disease. In the present study, we combined in silico (molecular docking as well as molecular dynamics) with in vitro studies to assess anti SARS-Cov-2 potential of setomimycin. According to the molecular docking study, setomimycin exhibited the best docking score with the M^{pro} enzyme among all the selected targets. Therefore, the in vitro studies were evaluated to determine the inhibitory potential of setomimycin against M^{pro}. It was found that setomimycin inhibits M^{pro} enzyme with an IC$_{50}$ value of 12.02 ± 0.046 μM. Additionally, anti-inflammatory and antioxidant properties of setomimycin were confirmed by ELISA assay, inhibition of nitric oxide, and DPPH assay, respectively. Overall, the findings suggest setomimycin as a potential COVID-19 therapeutics for COVID-19 disease and its related complications.

Declarations

Conflict of interest The authors have no relevant financial or nonfinancial interests to disclose.

References

1. Subbarao K, Mahanty S (2020) Respiratory virus infections: understanding COVID-19. Immunity 52:905–909. https://doi.org/10.1016/j.immuni.2020.05.004

2. Aldridge RW, Lewer D, Beale S, Johnson AM, Zambon M, Hayward AC, Fragaszy EB, Group FW (2020) Seasonality and immunity to laboratory-confirmed seasonal coronaviruses (HCoV-NL63, HCoV-OC43, and HCoV-229E): results from the Flu Watch cohort study. Wellcome Open Res. https://doi.org/10.12688/wellcomeopenres.15812.2

3. Yang Y, Yang Y, Peng F, Wang R, Guan K, Jiang T, Xu G, Sun J, Chang C (2020) The deadly coronaviruses: The 2003 SARS pandemic and the 2020 novel coronavirus epidemic in China. J Autoimmun 109:102434. https://doi.org/10.12688/wellcomeopenres.15812.2

4. Chen Z, Zhang W, Lu Y, Guo C, Guo Z, Liao C, Zhang X, Zhang Y, Han X, Li Q, Lu J (2020) From SARS-CoV to Wuhan 2019-nCoV outbreak: similarity of early epidemic and prediction of future trends. Available SSRN 3528722. https://doi.org/10.2139/ssrn.3528722

5. Alnuqaydan AM, Almutary AG, Sukamaran A, Yang BT, Lee XT, Lim WX, Ng YM, Ibrahim R, Darmarajan T, Nanjappan S, Chellian J (2021) Middle East Respiratory Syndrome (MERS) virus—pathophysiological axis and the current treatment strategies. AAPS PharmSciTech 5:1–23. https://doi.org/10.1208/s12249-021-02062-2

6. Zhu H, Wei L, Niu P (2020) The novel coronavirus outbreak in Wuhan, China. Glob Health Res Policy 5:1–3. https://doi.org/10.1186/s41256-020-00135-6

7. García-Basteiro AL, Chaccour C, Guinovart C, Llupià A, Brew J, Trilla A, Plasencia A (2020) Monitoring the COVID-19 epidemic in the context of widespread local transmission. Lancet Respir Med 8:440–442. https://doi.org/10.1016/S2213-2600(20)30162-4

8. Kim D, Lee JY, Yang JS, Kim JW, Kim VN, Chang H (2020) The architecture of SARS-CoV-2 transcriptome. Cell 181:914–921. https://doi.org/10.1016/j.cell.2020.04.011

9. Naqvi AA, Fatima K, Mohammad T, Fatima U, Singh IK, Singh A, Atif SM, Hariprasad G, Hasan GM, Hassan MI (2020) Insights into SARS-CoV-2 genome, structure, evolution, pathogenesis and therapies: Structural genomics approach. Biochim Biophys Acta Mol Basis Dis 1866:165878. https://doi.org/10.1016/j.bbadis.2020.165878

10. Fehr AR, Perlman S (2015) Coronaviruses: an overview of their replication and pathogenesis. Coronaviruses. https://doi.org/10.1007/978-1-4939-2438-7_1

11. Gong Y, Qin S, Dai L, Tian Z (2021) The glycosylation in SARS-CoV-2 and its receptor ACE2. Signal Transduct Target Ther 6:1–24. https://doi.org/10.1038/s41392-021-00809-8

12. Matheson NJ, Lehner PJ (2020) How does SARS-CoV-2 cause COVID-19? Science 369:510–511. https://doi.org/10.1126/science.abc6156

13. Silvestrini L, Belhaj N, Comez L, Gerelli Y, Lauria A, Libera V, Mariani P, Marzullo P, Ortore MG, Piccionello AP, Petrillo C (2021) The dimer-monomer equilibrium of SARS-CoV-2 main protease is affected by small molecule inhibitors. Sci Rep 11:1–6. https://doi.org/10.1038/s41598-021-88630-9

14. Klemm T, Ebert G, Calleja DJ, Allison CC, Richardson LW, Bernardini JP, Lu BG, Kuchel NW, Grohmann C, Shibata Y, Gan ZY (2020) Mechanism and inhibition of the papain-like protease, PLpro, of SARS-CoV-2. The EMBO J 39:e106275. https://doi.org/10.15252/embj.2020106275

15. Hilgenfeld R (2014) From SARS to MERS: crystallographic studies on coronaviral proteases enable antiviral drug design. FEBS J 281:4085–4096. https://doi.org/10.1111/febs.12936

16. Gao Y, Yan L, Huang Y, Liu F, Zhao Y, Cao L, Wang T, Sun Q, Ming Z, Zhang L, Ge J (2020) Structure of the RNA-dependent RNA polymerase from COVID-19 virus. Science 368:779–782. https://doi.org/10.1126/science.abb7498

17. Gil C, Ginex T, Maestro I, Nozal V, Barrado-Gil L, Cuesta-Geijo MÁ, Urquiza J, Ramírez D, Alonso C, Campillo NE, Martinez A (2020) COVID-19: drug targets and potential treatments. J Med Chem 63:12359–12386. https://doi.org/10.1021/acs.jmedchem.0c00606

18. Poduri R, Joshi G, Jagadeesh G (2020) Drugs targeting various stages of the SARS-CoV-2 life cycle: exploring promising drugs for the treatment of Covid-19. Cell Signal 74:109721. https://doi.org/10.1016/j.cellsig.2020.109721

19. Norrie JD (2020) Remdesivir for COVID-19: challenges of underpowered studies. Lancet 395:1525–1527. https://doi.org/10.1016/S0140-6736(20)31023-0

20. Anderson J, Schiffer C, Lee SK, Swanstrom R (2009) viral protease inhibitors. Antivir Strateg. https://doi.org/10.1007/978-3-540-79086-0_4

21. Hoffmann M, Hofmann-Winkler H, Smith JC, Krüger N, Arora P, Sørensen LK, Søgaard OS, Hasselstrøm JB, Winkler M, Hempel T, Raich L (2021) Camostat mesylate inhibits SARS-CoV-2 activation by TMPRSS2-related proteases and its metabolite GBPA exerts antiviral activity. EBioMedicine 65:103255. https://doi.org/10.1016/j.ebiom.2021.103255

22. Lin SH, Zhao YS, Zhou DX, Zhou FC, Xu F (2020) Coronavirus disease 2019 (COVID-19): cytokine storms, hyper-inflammatory phenotypes, and acute respiratory distress syndrome. Genes Dis. https://doi.org/10.1016/j.gendis.2020.06.009

23. Kumar SS, Binu A, Devan AR, Nath LR (2021) Mucus targeting as a plausible approach to improve lung function in COVID-19 patients. Med Hypotheses 156:110680. https://doi.org/10.1016/j.mehy.2021.110680

24. Fu B, Xu X, Wei H (2020) Why tocilizumab could be an effective treatment for severe COVID-19? J Transl Med 18:1–5. https://doi.org/10.1186/s12967-020-02339-3

25. Dong L, Hu S, Gao J (2020) Discovering drugs to treat coronavirus disease 2019 (COVID-19). Drug Discov Ther 14:58–60. https://doi.org/10.5582/ddt.2020.01012

26. Ojha PK, Kar S, Krishna JG, Roy K, Leszczynski J (2021) Therapeutics for COVID-19: from computation to practices—where we are, where we are heading to. Mol Divers. https://doi.org/10.1007/s11030-020-10134-x

27. Mohapatra S, Nath P, Chatterjee M, Das N, Kalita D, Roy P, Satapathi S (2020) Repurposing therapeutics for COVID-19: rapid prediction of commercially available drugs through machine learning and docking. PLoS ONE 15:e0241543. https://doi.org/10.1371/journal.pone.0241543

28. Muratov EN, Amaro R, Andrade CH, Brown N, Ekins S, Fourches D, Isayev O, Kozakov D, Medina-Franco JL, Merz KM, Oprea TI (2021) A critical overview of computational approaches employed for COVID-19 drug discovery. Chem Soc Rev. https://doi.org/10.1039/D0CS01065K

29. Wang Y, Li F, Zhang Y, Zhou Y, Tan Y, Chen Y, Zhu F (2020) Databases for the targeted COVID-19 therapeutics. Br J Pharmacol 177:4999–5001. https://doi.org/10.1111/bph.15234

30. Omura S, Tanaka H, Iwai Y, Nishigaki K, Awaya J, Takahashi Y, Masuma R (1978) A new antibiotic, setomimycin, produced by a strain of *Streptomyces*. J Antibiot 31:1091–1098. https://doi.org/10.7164/antibiotics.31.1091

31. Parthasarathi S, Sathya S, Bupesh G, Samy RD, Mohan MR, Kumar GS, Manikandan M, Kim CJ, Balakrishnan K (2012) Isolation and characterization of antimicrobial compound from marine *Streptomyces hygroscopicus* BDUS 49. World J Fish Mar Sci. https://doi.org/10.5829/idosi.wjfms.2012.04.03.5658

32. Rahalison LL, Hamburger M, Hostettmann K, Monod M, Frenk E (1991) A bioautographic agar overlay method for the detection of antifungal compounds from higher plants. Phytochem Anal 2:199–203. https://doi.org/10.1002/pca.2800020503

33. Jin Z, Du X, Xu Y, Deng Y, Liu M, Zhao Y, Zhang B, Li X, Zhang L, Peng C, Duan Y (2020) Structure of M pro from SARS-CoV-2 and discovery of its inhibitors. Nature 582:289–293. https://doi.org/10.1038/s41586-020-2223-y

34. Yan R, Zhang Y, Li Y, Xia L, Guo Y, Zhou Q (2020) Structural basis for the recognition of SARS-CoV-2 by full-length human ACE2. Science 367:1444–1448. https://doi.org/10.1126/science.abb2762

35. Kirchdoerfer RN, Ward AB (2019) Structure of the SARS-CoV nsp12 polymerase bound to nsp7 and nsp8 co-factors. Nat Commun 10:1–9. https://doi.org/10.1038/s41467-019-10280-3

36. Li Q, Wang Z, Zheng Q, Liu S (2020) Potential clinical drugs as covalent inhibitors of the priming proteases of the spike protein of SARS-CoV-2. Comput Struct Biotechnol J 18:2200–2208. https://doi.org/10.1016/j.csbj.2020.08.016

37. Sastry GM, Adzhigirey M, Day T, Annabhimoju R, Sherman W (2013) Protein and ligand preparation: parameters, protocols, and influence on virtual screening enrichments. J Comput Aided Mol Des 27:221–234. https://doi.org/10.1007/s10822-013-9644-8

38. Kim S, Chen J, Cheng T, Gindulyte A, He J, He S, Li Q, Shoemaker BA, Thiessen PA, Yu B, Zaslavsky L (2019) PubChem 2019 update: improved access to chemical data. Nucleic Acids Res 47:1102–1109. https://doi.org/10.1093/nar/gky1033

39. Li G, De Clercq E (2020) Therapeutic options for the 2019 novel coronavirus (2019-nCoV). Nat Rev Drug Discov 19:149–150. https://doi.org/10.1038/d41573-020-00016-0

40. Yin W, Mao C, Luan X, Shen DD, Shen Q, Su H, Wang X, Zhou F, Zhao W, Gao M, Chang S (2020) Structural basis for inhibition of the RNA-dependent RNA polymerase from SARS-CoV-2 by

remdesivir. Science 368:1499–1504. https://doi.org/10.1126/science.abc1560

41. Sonawane K, Barale SS, Dhanavade MJ, Waghmare SR, Nadaf NH, Kamble SA, Mohammed AA, Makandar AM, Fandilolu PM, Dound AS, Naik NM (2020) Homology modeling and docking studies of TMPRSS2 with experimentally known inhibitors Camostat mesylate, Nafamostat and Bromhexine hydrochloride to control SARS-Coronavirus-2. https://doi.org/10.26434/chemrxiv.12162360.v1

42. Rabbani G, Ahn SN, Kwon H et al (2021) Penta-peptide ATN-161 based neutralization mechanism of SARS- CoV-2 spike protein. Biochem Biophys reports 28:101170. https://doi.org/10.1016/j.bbrep.2021.101170

43. Struck A-W, Axmann M, Pfefferle S et al (2012) A hexapeptide of the receptor-binding domain of SARS corona virus spike protein blocks viral entry into host cells via the human receptor ACE2. Antiviral Res 94:288–296. https://doi.org/10.1016/j.antiviral.2011.12.012

44. LigPrep, Schrodinger, LLC, New York, USA

45. SiteMap, version 2.5, Schrödinger, LLC, New York, USA

46. Jockusch S, Tao C, Li X, Chien M, Kumar S, Morozova I, Kalachikov S, Russo JJ, Ju J (2020) Sofosbuvir terminated RNA is more resistant to SARS-CoV-2 proofreader than RNA terminated by Remdesivir. Sci Rep 10:1–9. https://doi.org/10.1038/s41598-020-73641-9

47. Picarazzi F, Vicenti I, Saladini F, Zazzi M, Mori M (2020) Targeting the RdRp of emerging RNA viruses: the structure-based drug design challenge. Molecules 25:5695. https://doi.org/10.3390/molecules25235695

48. Appleby TC, Perry JK, Murakami E, Barauskas O, Feng J, Cho A, Fox D, Wetmore DR, McGrath ME, Ray AS, Sofia MJ (2015) Structural basis for RNA replication by the hepatitis C virus polymerase. Science 347:771–775. https://doi.org/10.1126/science.1259210

49. Glide, version 5.7, Schrödinger, LLC, New York, USA

50. Bowers KJ (2006) Scalable algorithms for molecular dynamics simulations on commodity clusters. In: Proceedings of the 2006 ACM/IEEE conference on supercomputing, pp 43–43.https://doi.org/10.1109/SC.2006.54

51. Bakan A, Meireles LM, Bahar I (2011) ProDy: protein dynamics inferred from theory and experiments. Bioinformatics 27:1575–1577. https://doi.org/10.1093/bioinformatics/btr168

52. Humphrey W, Dalke A, Schulten K (1996) VMD: visual molecular dynamics. J Mol Graph 14(33–8):27–28. https://doi.org/10.1016/0263-7855(96)00018-5

53. Genheden S, Ryde U (2015) The MM/PBSA and MM/GBSA methods to estimate ligand-binding affinities. Expert Opin Drug Discov. https://doi.org/10.1517/17460441.2015.1032936

54. Tiwari H, Raina D, Gupta M, Barik MR, Khan IA, Khan F, Nargotra A (2021) Identification of novel MurA inhibitors using in silico approach, their validation and elucidation of mode of inhibition. J Biomol Struct Dyn. https://doi.org/10.1080/07391102.2021.2007793

55. Xie J, Schaich KM (2014) Re-evaluation of the 2, 2-diphenyl-1-picrylhydrazyl free radical (DPPH) assay for antioxidant activity. J Agric Food Chem 62:4251–4260. https://doi.org/10.1021/jf500180u

56. Bolt HM, Stewart JD (2012) Antioxidant activity of food constituents: relevance for the risk of chronic human diseases. Arch Toxicol 86:343–344. https://doi.org/10.1007/s00204-012-0812-8

57. Gulcin İ (2020) Antioxidants and antioxidant methods: an updated overview. Arch Toxicol 94:651–715. https://doi.org/10.1007/s00204-020-02689-3

58. Hatada R, Okuwaki K, Mochizuki Y, Handa Y, Fukuzawa K, Komeiji Y, Okiyama Y, Tanaka S (2020) Fragment molecular orbital based interaction analyses on COVID-19 main protease-inhibitor N3 complex (PDB ID: 6LU7). J Chem Inf Model 60:3593–3602. https://doi.org/10.1021/acs.jcim.0c00283